High momentum components in nuclei

M. Avan, A. Baldit, J. Castor, M. El Zoubidi, J. Fargeix, H. Fonvieille, P. Force, J. L. Guelou, B. Harradi, and G. Landaud
Laboratoire de Physique Corpusculaire, Université de Clermont II, 63170 Aubiere, France

J. P. Didelez and F. Reide
Institut de Physique Nucléaire, 91406 Orsay, France

M. Bernheim, A. Gerard, A. Magnon, C. Marchand, J. Morgenstern, J. Picard, and P. Vernin
Departement de Physique Nucléaire, Centre d'Etudes Nucléaires de Saclay, Gif-sur-Yvette, France

H. Jackson
Argonne National Laboratory, Argonne, Illinois
(Received 22 April 1987)

To clarify the analysis of our existing backward proton scattering data in terms of high momentum components in nuclei, we have measured exclusive cross sections for the backward energetic protons in coincidence with the γ rays emitted by the target. At 200 MeV incident proton energy, the mass distribution of the residual nuclei from a ^{28}Si target suggests a single scattering reaction on a nucleon of the target. We have also performed large momentum transfer electron scattering on ^{12}C and ^{58}Ni using a 640 MeV electron beam. These data analyzed within the quasi-two-body scaling approach display a scaling regime identical to the one previously observed for the protons. Both of these features give credence to the "single scattering," basic assumption in the quasi-two-body scaling theory. The experimental momentum distribution is in good agreement with several theoretical predictions which include short range correlations.

I. INTRODUCTION

A few years ago, it was suggested that the backward scattering of energetic protons could be directly related to the high momentum components of nucleons in nuclear matter.[1] In the framework of the quasi-two-body scaling (QTBS) approach, much of the data could be fitted using a universal momentum density which had a tail extending as far as 1 GeV/c.[2,3] Gurvitz, using a refined theory including final state interactions, shows that, above 300 MeV/c, the deduced nucleon momentum distribution in nuclei is universal, independent of the projectile or the target for all data taken with projectile energies larger than 600 MeV/nucleon.[4]

We have measured inclusive cross sections[5] for energetic protons emitted at large angles, using the 200 MeV ORSAY synchrocyclotron proton beam on ^{27}Al, ^{58}Ni, and ^{197}Au targets. These data scale perfectly, but the scaling regime is drastically different from the one observed at higher incident energies. The population of high momenta is much smaller,[5] and we have already argued that our lower energy data give more reliable information because the multiple scattering in nuclei is less severe at 200 MeV, where the N-N cross sections are smaller. Moreover, for the highest incident energies large momenta are artificially generated in the QTBS approach in which neither the inelastic processes nor the distortion of the projectile are taken into account.[6]

Recently, we have recorded exclusive spectra (p-γ coincidences), using 200 MeV protons scattered by a ^{28}Si target.[6,7] The γ spectra lead to the distribution of the residual nuclei, which in turn, is the reflection of the excitation energy transferred to the target. This energy presents a peak in the 10 MeV region, indicating that the reaction mechanisms involve a small number of interactions. Hence, the "single scattering" assumption, which is the most critical one in the QTBS approach,[7] seems credible.

Electron experiments can fundamentally demonstrate this last point, because electrons undergo only single scattering. Our electron data using the 640 MeV Saclay electron beam, when analyzed in the QTBS framework, display a scaling regime identical to the one observed with the 200 MeV protons, favoring again our lower energy proton approach.

Finally, in order to understand the discrepancy between proton results taken at different incident energies, we have simulated the backward proton scattering with Monte Carlo cascade codes. It shows that the production of pi mesons plays a major part in generating significant back angle cross sections for projectile energies larger than 300 MeV/nucleon.

II. EXPERIMENTAL RESULTS

A. Proton γ coincidences

The experimental setup recently described[8,9] was the major equipment in our early (p-γ) coincidences investi-

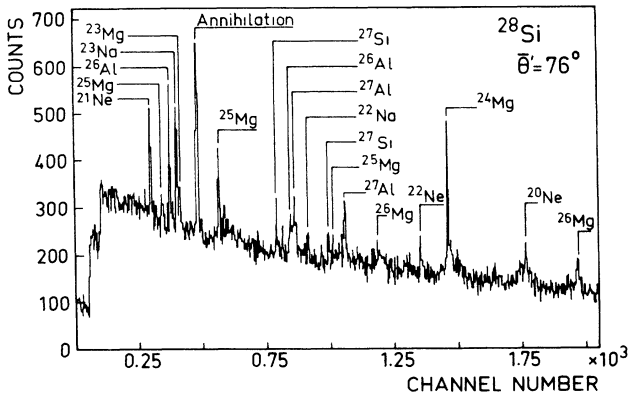

FIG. 1. (p-γ) coincident spectrum showing the photopeaks corresponding to several residual nuclei. The coincident protons were emitted at 76° lab with an energy larger than 80 MeV.

gations.[10] Coincident (p-γ) events triggered the data-taking system which recorded correlated proton and gamma energy spectra. The γ-ray detector was a high purity Ge(Li) (150 cm^3) viewing the ^{28}Si target with a solid angle of 0.12 sr at 120° from the beam direction. Only protons with energies larger than 80 MeV were detected at an average angle of 76° by a large acceptance (angle and energy) magnetic spectrometer.

A typical γ spectrum is shown in Fig. 1. Several peaks can be identified on a large Compton background and related through known decay schemes to given residual nuclei. The relative population of those residual nuclei is summarized in Table I, where it can be seen that the removal of one to eight nucleons from the target could be traced. In practice, for each nucleus, we search only the γ-ray peaks corresponding to transitions through the first or the second excited states. We select a γ peak if its energy E_γ corresponds to a tabulated energy E_γ^t within $|E_\gamma - E_\gamma^t| \leq 2$ KeV.

Using such a procedure, direct transitions from a high excitation level to the ground state are not counted. The corresponding inefficiency can be estimated considering the branching ratios in the decay schemes and is of the order of 30% or even larger since high excitation levels usually correspond to a high level density region. In Table I, we give for each residual nucleus the relative population which suffers negligible effects from the selection procedure described above.[7]

The Compton background lying under the photoelectric peaks was subtracted using a standard procedure as outlined in Ref. 10.

It can be seen that residual nuclei corresponding to the removal of one nucleon from the target, namely, ^{27}Al and ^{27}Si, represent 26% of the total population. The ratio between ^{27}Al* and ^{27}Si* is consistent with the ratio of the 90° differential cross sections p-p and p-n at 200 MeV in the center of mass.

TABLE I. Relative population of residual nuclei.

Residual nucleus	$\frac{\sigma_i(\text{p-}\gamma)}{\sum_i \sigma_i(\text{p-}\gamma)}$
^{28}Si	0
^{27}Si	9,4
^{27}Al	16,6
etc.	etc.

On the other hand, there is no ^{28}Si* in the γ spectrum. Our previous (p-γ) coincidence experiment at 400 MeV incident proton energy,[10] had shown indeed that coherent inelastic scattering decreases very *quickly* with the scattered proton angle. This also justifies the choice of 76° as representative of the "back-angle" situation in a coincidence experiment for which a compromise has to be made to keep counting rates (four coincidences/s) and statistical accuracy within reasonable limits.

To find a high energy proton at a large angle, at least one nucleon must be ejected and the initial stage of the process is

$$p + {}^{28}\text{Si} \rightarrow \begin{cases} {}^{27}\text{Al}^* + p' + p'' \\ {}^{27}\text{Si}^* + p' + n'' \end{cases} . \quad (1)$$

As usual in the quasifree scattering terminology, the intermediate ^{27}Al* or ^{27}Si* nuclei can be considered as "spectator nuclei." If their excitation energy is large enough, they can evaporate particles before becoming the final residual nucleus from which the coincident γ-ray will be emitted.

From this realistic view of the mechanism, we calculate the excitation energy E_x produced in the reaction. The evaporation code Alice[11] determines the probabilities to detect a given final nucleus by evaporation from ^{27}Si* or ^{27}Al* intermediate spectator nuclei. These probabilities are directly connected to the initial energy E_x. The relative population of the final residual nuclei is given in Table I and a convolution with the probabilities of evaporation leads to the distribution of the excitation energy in the reaction $p + {}^{28}\text{Si} \rightarrow p' + X$. The complete calculation is outlined in Ref. 7 and the result is displayed in Fig. 2. This spectrum is strongly peaked at

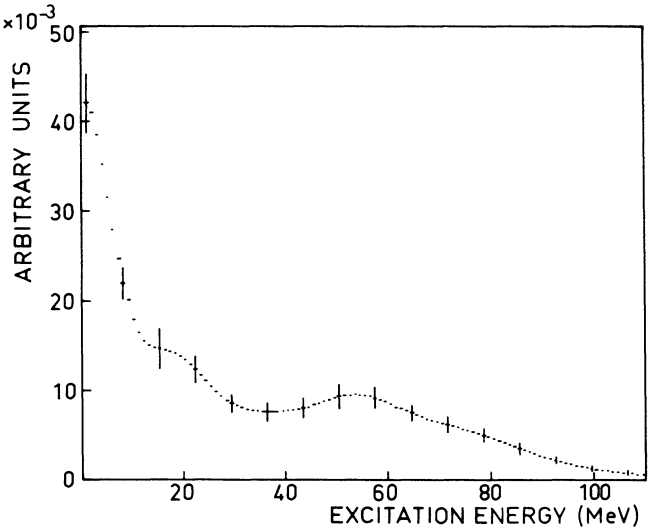

FIG. 2. Distribution of the excitation energy transferred by the incident proton being scattered at 76°. Error bars reflect statistical uncertainties on the original γ spectra.

low energy which means that low dissipative processes are the most probable. The large angle scattering of the incident proton is mainly achieved by a single scattering on one nucleon, leaving the $A-1$ spectator fragment rather cold. On the contrary, if the detected proton was issued from a series of "small angle scattering" on several target nucleons, the energy would have been thermalized in each step. The broad peak at 50 MeV in Fig. 2 can be partly explained by such cascade processes. In fact, we detect a proton which keeps the major part of the incident kinetic energy and leaving a struck nucleon in the target which has a large probability to start an intranuclear cascade (FSI), the fast back scattered particle remaining unperturbed.

To validate the study of the (p-γ) coincidence, our proton spectrum (Fig. 3) summed on all residual nuclei of Table I is compared with the inclusive spectrum. Both have comparable shapes and can be related to the same scattering mechanism. However, coincident cross sections represent 20% of the inclusive ones. We argue that the ground state transition for the spectator nuclei cannot emit a γ ray. On the other hand, high energy γ transitions are not identified; they do not cascade through the first or second excited state of the residual nuclei, and the photoelectric efficiency of the Ge detector is small for $E_\gamma > 2$ MeV.

More precisely, the Ge detector efficiency has been simulated by a Monte Carlo program taking into account photoelectric, Compton, and pair production processes. For the identified peaks leading to the distribution outlined in Table I, we have calculated and summed the corresponding Compton spectra (Fig. 4). The result

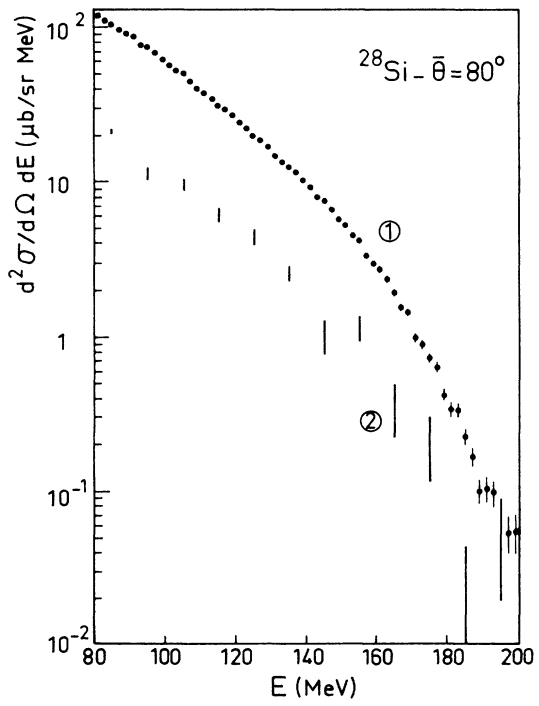

FIG. 3. (1) Inclusive and (2) exclusive proton cross sections vs outgoing proton energy. The exclusive spectrum is a sum over all residual nuclei of Table I.

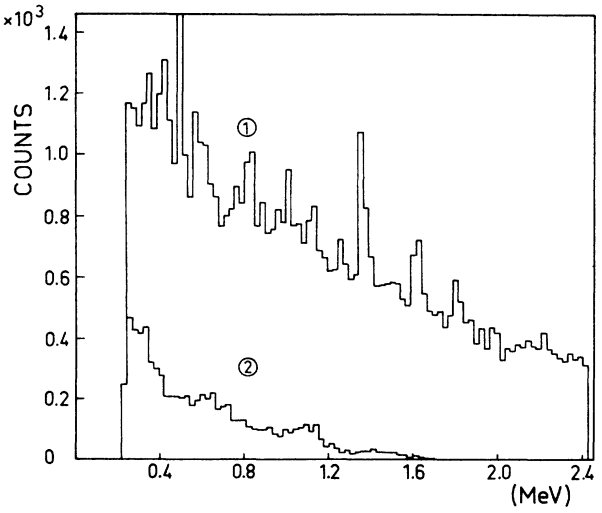

FIG. 4. (1) Experimental (p-γ) spectrum. (2) Monte-Carlo simulation of Compton background.

represents only 20% of the experimental Compton spectrum observed below 2 MeV. In addition, the level of the experimental background above 2.5 MeV generated by unidentified high energy γ-ray transitions is high.

The calculated Compton efficiency of the Ge diode for γ rays between 2 and 10 MeV happens to be rather independent of the initial γ energy and averages to 3.5×10^{-3}. We can therefore estimate the proton cross sections $d^2\sigma/d\Omega\, dE$ from the coincident spectra summed on all detected γ rays, each with its own efficiency (Compton or photoelectric). Figure 5 shows the comparison between the coincident cross sections and the inclusive cross sections; the overall agreement is quite good.

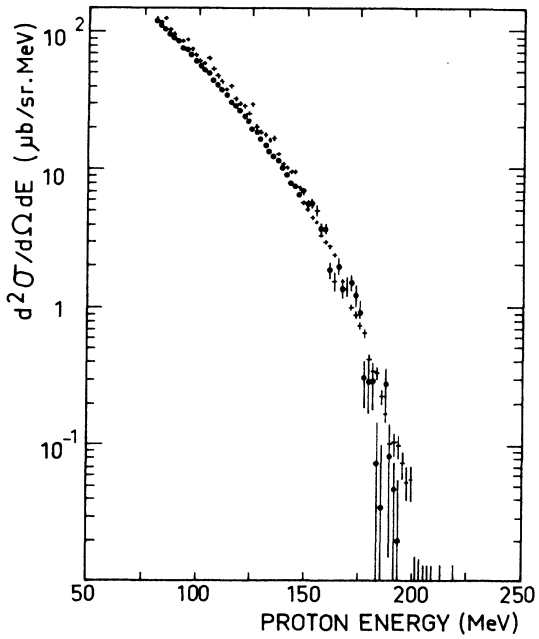

FIG. 5. Comparison between inclusive proton cross section and γ-coincident proton cross sections after the efficiency corrections outlined in the text. (●) Inclusive cross section; (+) coincident cross section.

TABLE II. Targets and kinematical conditions.

Targets	Angles	Incident energies (MeV)
^{58}Ni	120°	642
^{12}C	120°	642
^{12}C	75°	642
^{12}C	145°	421

B. Electron scattering

1. Introduction

The interest in electrons as a probe of nuclear matter is obvious because they undergo only single scattering. Unfortunately, there are almost no published inclusive data for $e+A \rightarrow e'+X$ in the kinematical region of interest and for targets with $A > 4$.[12] The experimental facility existing at the Saclay Linear Accelerator allowed us to measure the electron scattering cross section in kinematical conditions corresponding to large momentum transfer (~ 1 GeV/c). One can thus reach values of the scaling kinematical variable comparable to the ones explored before with protons (~ 400 MeV/c). The incident electron had an energy of 640 MeV and bombarded a ^{12}C and a ^{58}Ni targets;[13] inclusive cross sections for scattered electrons were recorded with four kinematical conditions listed in Table II.

Scattered electrons were selected by the "600 MeV/c" magnetic spectrometer (momentum range: 40%, solid angle: 6.5 msr, intrinsic resolution: 4×10^{-4}). The focal plane is equipped with multi-wire proportional chambers (MWPC), plastic scintillators, and threshold gas Cherenkov detectors. Beam monitoring was accomplished by use of a Faraday cup and an induction ferrite core with a precision of 1%.

The smallest cross sections were also measured with the "900 MeV/c" magnet which has a better signal to background ratio (momentum acceptance: 9%). Figure 6 illustrates the good overlap between cross sections measured by the two magnets.

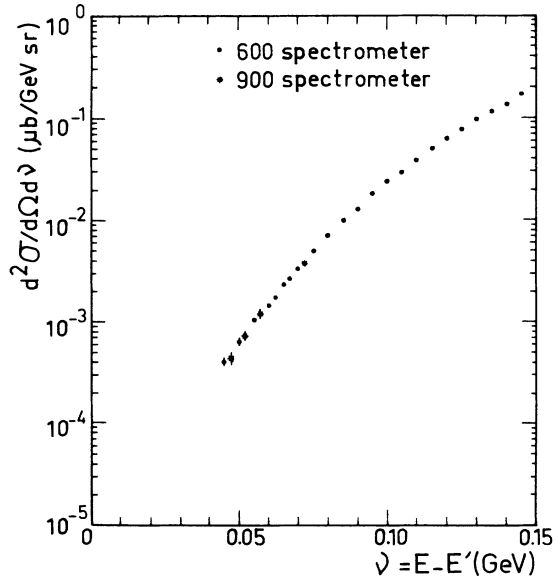

FIG. 6. Electron differential cross sections obtained with the two spectrometers: "900 MeV/c" and "600 MeV/c."

2. Radiative corrections

In the particular case under investigation in this paper, the contribution of radiative tail is small. The correction for the continuum is tracked by the peaking approximation. The correction procedure is the one of Tsai (Ref. 14) and is developed in detail in Ref. 15. In the region of the largest momentum transfer it can change the overall normalization by 30% at most. Figure 7 shows the electron spectra after radiative corrections.

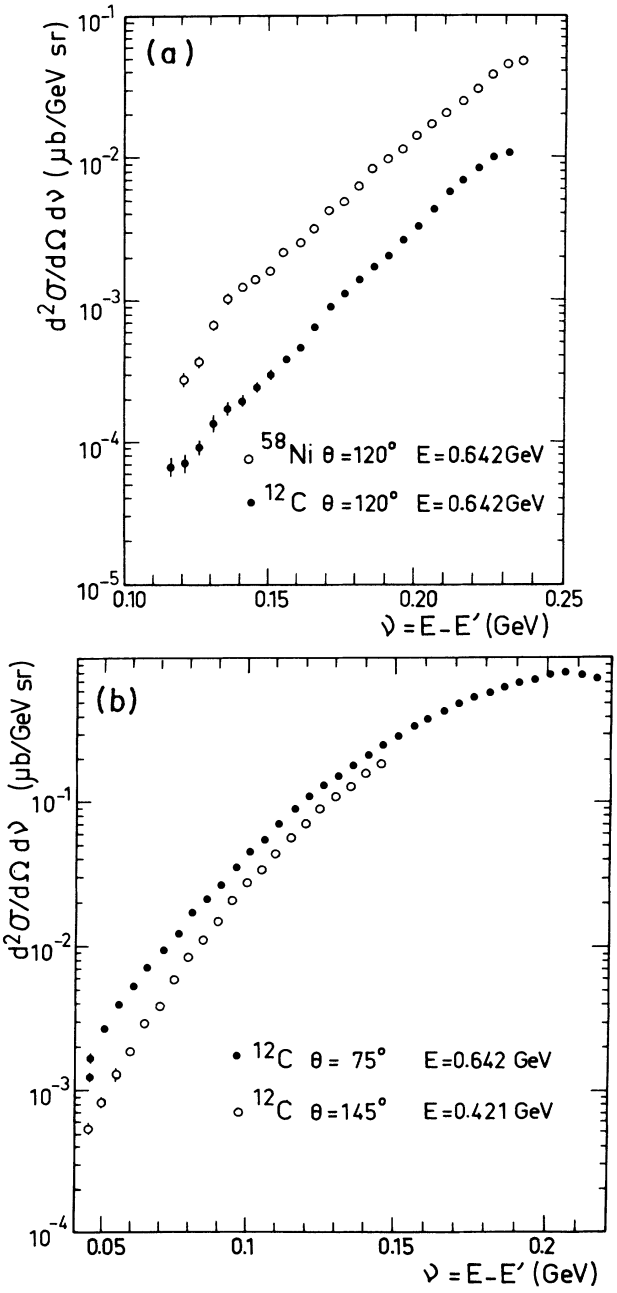

FIG. 7. Scattered electron spectra: (a) from ^{58}Ni and ^{12}C targets at $\theta=120°$, $E=0.642$ GeV, and (b) from ^{12}C at $\theta=75°$, $E=0.642$ GeV and $\theta=145°$, $E=0.421$ GeV.

3. *Inclusive cross sections*

To transform inclusive cross sections in the scaling representation we have used only this part of the e′ spectrum corresponding to target excitation energies higher than the giant quadrupole resonance (to avoid coherent scattering) and smaller than 140 MeV to forbid elementary inelastic processes (π electroproduction). The corresponding cross sections are displayed on Fig. 8 in our QTBS scaling representation and compared with those of protons.

The maximum $k_{\min}$ reached with electrons is 400 MeV/c (versus 450 MeV/c with protons) and in the overlap region 300–420 MeV/c, the scaling is identical for protons and electrons (same response function from the target nucleus) as will be described in more detail in Sec. III. With the ^{12}C target, we have recorded data at $\theta=75°$, which corresponds to a $k_{\min}$ range of 170 to 300 MeV/c.

III. THEORETICAL ANALYSIS

The scaling representation for electron data is based on the same picture as the one used previously for protons.[5] If a projectile is scattered at large angle with small energy loss after a single scattering on a nucleon of the target, this target nucleon must have had before the collision a large Fermi momentum. Pure kinematical relation fix a minimum value of this momentum ($k_{\min}$). In the QTBS picture, the backward scattering cross sections can be related to the probability that the target nucleon has a Fermi momentum larger than $k_{\min}$. The single scattering approximation is a dominant feature of the QTBS and is certainly justified in the case of electrons scattering (the effect of Coulomb distortion is of the order of a few percent on cross sections). Even for hadrons scattering, the QTBS approach ignores rescattering of the projectile on target nucleons. However, other effects such as the final state interaction of nuclear fragments, binding potential effects in the scattering on bound nucleon, and, if necessary, Pauli interchange effects are taken into account.[3,4] The experimental inclusive cross sections can be expressed in terms of on-shell projectile nucleon cross sections. In the case of electrons, the cross sections are

$$\frac{d^2\sigma_{eA\to e'X}}{dE_{e'}d\Omega_{e'}}=\frac{m(p_L^{\rm eff})^2}{4\pi^2}\frac{p'}{p}\left[Z\frac{d\sigma_{ep}}{dq^2}(E_L^{\rm eff},q^2)+(A-Z)\frac{d\sigma_{en}}{dq^2}(E_L^{\rm eff},q^2)\right]\frac{G(k_{\min})}{|\mathbf{p}-\mathbf{p}'|}\ . \tag{2}$$

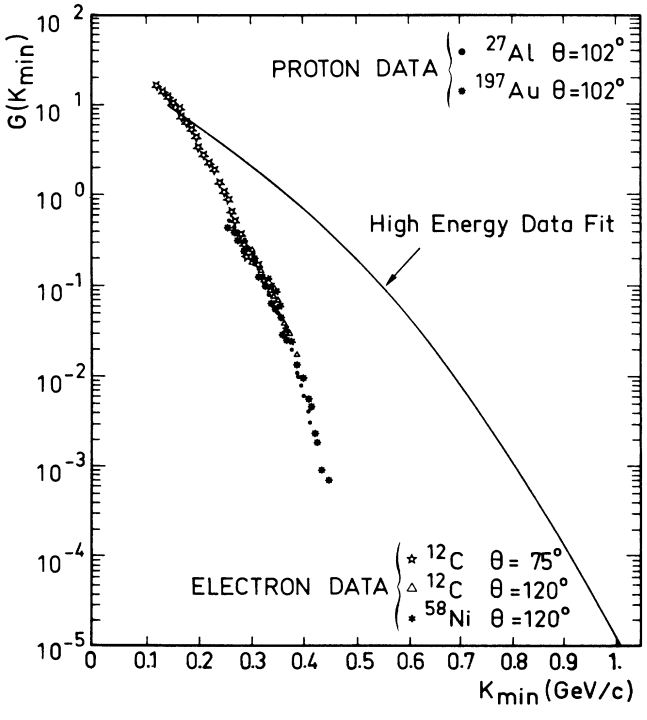

FIG. 8. The integrated distributions $G(k_{\min})$ as a function of the scaling variable $k_{\min}$ for our proton and electron data. The solid curve is the $G(k_{\min})$ extracted from the high energy proton data fit.

The quantity $G(k_{\min})$ is defined as

$$G(k_{\min})=\frac{1}{\pi}\int_{k_{\min}}^{\infty}k\,n(k)dk\ , \tag{3}$$

and is the integrated one nucleon momentum distribution. Here, $n(k)$ is normalized as $\int n(k)d^3k/(2\pi)^3=1$. The momentum $k_{\min}$ is the minimal momentum of the struck nucleon N in the reaction

$$e+N\to e'+N'\ , \tag{4}$$

where the struck nucleon (and the projectile) are on the mass shell before and after the collision.[4] It is easy to obtain the minimum value of $|\mathbf{k}_N|=|\mathbf{k}_{\min}|$, namely,

$$|\mathbf{k}_{\min}|=\left|\frac{\mathbf{q}}{2}\left[1-\frac{\nu}{|\mathbf{q}|}\left[1+\frac{4m^2}{\mathbf{q}^2-\nu^2}\right]^{1/2}\right]\right|\ ,$$

where $\mathbf{q}=\mathbf{p}-\mathbf{p}'$ and $\nu=E-E'$ are the momentum and energy transfers from projectile to the nucleus and $\mathbf{p}$ and $\mathbf{p}'$ are the initial and final momenta of the projectile in the laboratory frame, $|\mathbf{q}|$ and ν are typically $\sim$0.9 GeV/c and $\sim$100 MeV, respectively. The electromagnetic nucleon form factors used for the electron data are given by Höhler *et al.*[16]

All details concerning the theoretical approach are given in Refs. 4 and 5. The integrated momentum distribution $G(k_{\min})$ is directly extracted from the data and plotted as a function of $k_{\min}$. The scaling in $k_{\min}$ variable means that $G(k_{\min})$ extracted from different sets of

data fits the same curve.

The integrated distributions extracted from our data and corresponding to the different targets used in our experiments are plotted on Fig. 8 and compared to other projectile data.[5] Points corresponding to protons on ^{27}Al, ^{58}Ni, and ^{197}Au, and electrons on ^{58}Ni and ^{12}C, are perfectly aligned indicating that the same scaling regime is established in both cases.

IV. DISCUSSION

The basic assumption of the QTBS concept is that cross sections at backward angles are dominated by a single projectile nucleon collision. The projectile is scattered at large angle with small energy loss while the low energy nucleon (forward scattered) interacts with the residual nucleus (FSI). This approach ignores the multiple scattering of the backward emitted particle; the question is to know if this is legitimate.

The data obtained with electrons provide a straightforward answer since electrons undergo only single scattering. Actually, we see, on Fig. 8, that electron data are perfectly aligned with our proton data up to $k_{\min}=400$ MeV/c. This result confirms the dominance of the single scattering assumption for proton energies less than $\sim$300 MeV. In contrast, at 0.6–1 GeV incident energy, the reaction mechanism is drastically different. The threshold for π production is exceeded and the total p-p cross section has a broad maximum corresponding to the excitation of the $\Delta(1232)$ resonance in the nucleon-nucleon subsystem. For example, at 800 MeV, the inelastic channel is as probable as the elastic one. Not only is the mean-free-path in nuclear matter considerably reduced, but π production is allowed and very likely occurs. The elementary N-N scattering produces a three body final state (N-N-π) which is described in the QTBS approach by an elastic on-shell (N-N) cross section and kinematical variables corresponding to a two body (N-N) final state. In comparison, at 200 MeV, the N-N cross section is at a minimum; protons have therefore a large mean-free-path, and because of the small energy loss, no π can be produced. In view of the above, we are convinced of the QTBS theory only for those experimental data corresponding to global energy losses smaller than the π mass. Otherwise the values of $G(k_{\min})$ are not reliable. One should notice that for most data taken at high incident energies, large energy losses (greater than π mass) are allowed, the detected particles having at most half of the energy of the incident ones. This is generally true except for very light target nuclei, but in this particular case, the $G(k_{\min})$ extracted from the data does not follow the universal law.[4] Our electron data plotted in Fig. 8 correspond to energy losses smaller than the π mass, so that only elastic $d\sigma_{eN}$ cross sections have to be used in relation[2] to extract the $G(k_{\min})$.

To check the idea that the difference between $G(k_{\min})$ distribution in the range 0.6–1 GeV and at 200 MeV incident energies is primarily induced by π production, we have run the cascade code developed by Cugnon, in which inelastic channels are taken into account.[17] We obtain in the range 0.6–1 GeV a good simulation of the "experimental inclusive cross section." On the other hand, we have used a cascade code with only N-N elastic cross sections. This second code is a special version of the code Vegas[18] requiring small computing times. The results of those simulations are displayed in Fig. 9 in the scaling representation for 600 MeV protons incident on ^{27}Al. It is clear that the inclusion of inelastic channels is necessary to reproduce qualitatively the "universal" $G(k_{\min})$ which, by the way, can be generated without the need of particularly large internal momenta for the struck nucleon.

In a recent preprint,[19] inclusive proton cross sections at backward angles have been measured at 300 MeV incident energy. We first note that the scaling regime is identical to the one we have found at 200 MeV, as expected from the arguments developed above.

Analyzing power A_y as a function of outgoing proton energy has also been measured at large angles with Be and C targets. For a pure single scattering mechanism, the measured A_y should be strongly correlated with the A_y evaluated for p-N scattering at the proper momentum and energy. Such an evaluation has been done in Ref. 19 and predicts negative value of the order -0.1 to -0.3. It is an essential result of Ref. 19 that for energetic protons at backward angles [$E_p >$ (kinematical limit minus 70 MeV)], those values are rather well reproduced. Error bars are large for those particular events, but the general tendency is clear. So in this restricted phase-space region, A_y measurements also argue in favor of the "single scattering" approximation.

It is an approximation, however, meaning that among the few interactions which occur, only the large angle scattering on a large internal momentum target nucleon can generate an energetic proton at backward angle and dominates the inclusive cross sections. The neglected few small angle scatters can flip the projectile spin and might have a more drastic effect on asymmetries than on inclusive cross sections. Our γ-proton coincidence re-

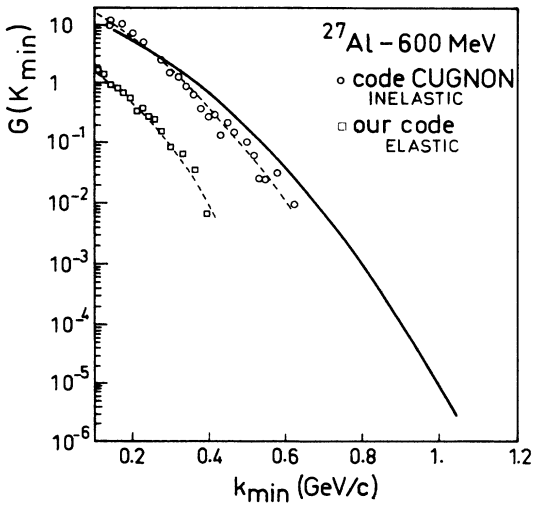

FIG. 9. $G(k_{\min})$ simulated by cascade codes for 600 MeV protons on ^{27}Al. Solid curve: same meaning as in Fig. 8.

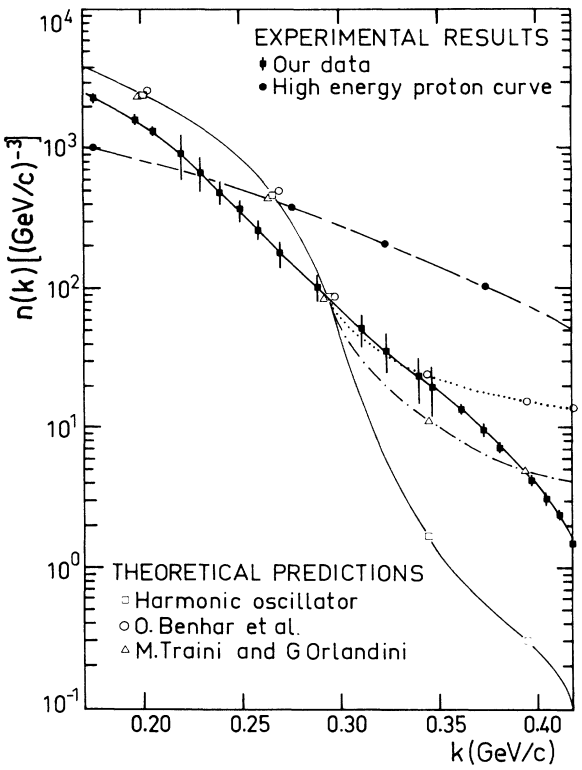

FIG. 10. Experimental one nucleon momentum distribution: ■ the solid curve results from a fit of all our proton and electron data; (0,300 GeV/c−0,420 GeV/c: proton and electron data; 0,170 GeV/c−0,300 GeV/c: electron data only). A few points with error bars are selected to show the experimental statistical errors. ● high energy proton curve. Theoretical predictions for ^{40}Ca: □ Harmonic oscillator, ○ Benhar *et al.* (Ref. 23), and △ Traini and Orlandini (Ref. 24).

sults have also demonstrated directly the dominance of simple reaction mechanisms for large angle scattering but show also that the detail of the reality is not that simple.

V. CONCLUSIONS

In conclusion, we claim that our backward angle inclusive proton spectra are good candidates to match the theoretical framework of QTBS, while, in contrast, data taken at higher incident energy are not. Our 200 MeV proton data and electron data provide the same $G(k_{\min})$, justifying *a posteriori*, the dominance of the single scattering mechanism as a basic assumption of QTBS. In addition, the (p-γ) coincidence spectra show that low dissipative processes still dominate the large angle scattering suggesting a mechanism involving a small number of interactions. As a rule, in the present status of the QTBS theory, the analysis should be restricted to inclusive scattering data corresponding to small energy losses; in any case, smaller than the π mass. We stress that such is the case for our proton and electron experimental results described in the present paper.

The data analysis in the framework of Gurvitz's latest version of the QTBS theory (in which the final state interaction was explicitly taken into account[4] provides the integrated distributions of $G(k_{\min})$. Having the integrated distributions $G(k_{\min})$ as a function of $k_{\min}$ [relation (3)], it is easy to derive the corresponding one nucleon momentum distribution $n(k)$, where k is the momentum of the struck nucleon before the shock. Figure 10 gives $n(k)$ for 170 MeV/$c \leqq k \leqq$ 420 MeV/c. The extent to which $n(k)$ can be considered as the actual one nucleon momentum distribution relies heavily on the quality of the theoretical treatment in QTBS; in particular the validity of the Optimal Approximation, the correct treatment of the FSI and the choice of the scaling variable.[20,21] We have attempted however to compare $n(k)$ to theoretical predictions as calculated in Refs. 22–24.

In those approaches, the momentum distribution $n(k)$ is the sum of a "single particle" part and a "correlation" part. Beyond a momentum of about 300 MeV/c, the "correlation" part becomes large and rapidly dominates the single particle contribution.

In Fig. 10, our $n(k)$ is plotted against the calculated ones for ^{40}Ca. The theoretical curves have been reproduced from figures of Refs. 23 and 24 after multiplication by appropriate factors to take into account different normalization prescriptions. Also plotted is the $n(k)$ deduced from high energy data fit. Although our experimental $n(k)$ displays much less high momentum components as inferred from the higher energy proton data, it is seen from Fig. 10 that beyond 350 MeV/c, it is roughly an order of magnitude higher than the independent particle contribution (harmonic oscillator), and in qualitative agreement with the additional contribution generated by short range correlations. We note that the present choice of the scaling variable minimizes the amount of high momentum components compared to previous prescriptions.[3] On the other hand, our electron data provide an indication on the behavior of $n(k)$ at lower momenta, namely, 170 MeV/$c \leqq k \leqq$ 300 MeV/c. The agreement with theoretical curves is satisfactory.

ACKNOWLEDGMENTS

We wish to thank Professor S. A. Gurvitz for his help in the theoretical analysis of this experiment. He has also suggested the electron experiment for $k_{\min} \geq 300$ MeV/c. The Orsay Synchrocyclotron and Saclay Linear Accelerator crews are acknowledged for their dedication to running the machine during all experiments.

[1]S. Frankel, Phys. Rev. Lett. **38**, 1338 (1977).
[2]S. Frankel *et al.*, Phys. Rev. C **18**, 1375 (1978); S. Frankel, W. Frati, R. H. Woloshyn, and D. Young, *ibid.* **18**, 1379 (1978).
[3]S. A. Gurvitz, Phys. Rev. Lett. **47**, 560 (1981).
[4]S. A. Gurvitz, Weizmann Institute of Science, Report No. WIS 82/7/March-PH, 1982; S. A. Gurvitz, Phys. Rev. C **33**, 422 (1986).
[5]M. Avan *et al.*, Phys. Rev. C **30**, 521 (1984).
[6]M. Avan *et al.*, International Symposium on Nuclear Spectroscopy and Nuclear Interactions, Osaka, 1984 (unpublished); M. Avan *et al.*, Proceedings of the COPECOS Workshop, Bad Honnef, Germany, 1984, edited by H. Machner and P. John (World Scientific, Singapore, 1985), pp. 80–92.
[7]P. Force, thèse d'Etat, Série E, No. 370, Université de Clermont II, France, 1986.
[8]J. Yonnet *et al.*, Phys. Rev. Lett. **40**, 164 (1978).
[9]C. Lebrun *et al.*, Nucl. Instrum. Methods **165**, 409 (1979).
[10]G. Landaud *et al.*, Nucl. Phys. **A384**, 323 (1982).
[11]M. Blann, Overland Alice, Report No. C-00-3494-29, Julich-Bonn University, 1976.
[12]S. V. Dementiy, Yad. Fiz. **37**, 621 (1983) [Sov. J. Nucl. Phys. **37**, 370 (1983)].
[13]M. Avan *et al.*, in XIth Europhysics Divisional Conference, Paris, 1985 (unpublished).
[14]Y. S. Tsai, Stanford Linear Accelerator Center, Report No. SLAC-PUB-848, 1971; L. W. Mo and Y. S. Tsai, Rev. Mod. Phys. **41**, 20 (1969).
[15]B. Harradi, thèse de 3ème, Cycle No. 870, Université de Clermont II, France, 1986.
[16]G. Höhler *et al.*, Nucl. Phys. **B114**, 505 (1976).
[17]J. Cugnon, T. Nizutani, and J. Vandermeulen, Nucl. Phys. **A352**, 505 (1981).
[18]K. Chen, Z. Fraenkel, G. Friedlander, J. R. Grover, J. M. Miller, and Y. Shimamoto, Phys. Rev. **166**, 949 (1968); H. W. Bertini, Phys. Rev. **131**, 1801 (1963).
[19]A. Moalem *et al.*, in TRIUMF, Report No. 86-f-visitor, Moalem, 1986.
[20]S. A. Gurvitz, J. A. Tjon, and S. J. Wallace, Phys. Rev. C **34**, 648 (1986); S. A. Gurvitz and A. Rinat, Weizmann Institute of Science, Report No. WIS 86/92/June-PH.
[21]Ciofi Degli Atti, in *Proceedings of the Theoretical and Experimental Investigation of Hadronic Few-Body Systems,* edited by C. Ciofi Degli Atti, O. Benhar, E. Pace, and G. Salme (Springer-Verlag, Berlin, 1986).
[22]J. G. Zabolitzky and W. Ey, Phys. Lett. **76B**, 527 (1978).
[23]O. Benhar *et al.*, in *Proceedings of the 2nd Workshop on Perspective in Nuclear Physics at Intermediate Energies,* ICTP, Trieste, 1985 (World Scientific, Singapore, 1985).
[24]M. Traini and G. Orlandini, Z. Phys. (in press).